Bulgarian Chemical Communications, Volume 48, Number3 (pp. 469– 475) 2016

Hydrogen sorption of magnesium plates deformed by surface mechanical attrition treatment

Á. Révész[1*], C. Szilágyi[1], T. Spassov[2]

[1]*Department of Materials Physics, Eötvös University, Budapest, H-1518, P.O.B. 32, Budapest, Hungary*
[2]*Faculty of Chemistry and Pharmacy, University of Sofia "St. Kl. Ohridski", 1 J. Bourchier Str., 1164 Sofia, Bulgaria*

Received June 26, 2015; Revised December 1, 2015

Surface modification attrition treatment was carried out on commercial magnesium disks in a SPEX 8000 shaker mill. Morphological and microstructural evolution during the severe plastic deformation process have been investigated by scanning electron-microscopy and X-ray diffraction line profile analysis, respectively. Complementary hydrogen absorption experiments in a Sieverts'-type apparatus revealed that hydrogen kinetics and the microstructural parameters exhibit correlation.

Keywords: Hydrogen storage; Mg-based; Microstructure; Severe plastic deformation; Surface modification by attrition treatment.

INTRODUCTION

Magnesium attracts high interest in solid state hydrogen storage due to its remarkable gravimetric storage capacity, lightness and moderate cost [1, 2]. Unfortunately, the relatively high stability of the hydride phase and the poor $Mg \leftrightarrow MgH_2$ kinetics retain the wide-spread application of commercial MgH_2 [3]. In order to overcome these obstacles, magnesium is extensively subjected to severe plastic deformation (SPD) by different technical routes [4, 5]. Among them high energy ball milling (HEBM) is applied, since this technique leads to the most effective particle-size and crystallite-size reduction [3, 6-8], which significantly enhance the hydrogen sorption kinetics due to the increased volumetric density of grain boundaries and lattice defects [9, 10]. Moreover, the addition of metal or metal-oxides catalyst powders to magnesium [9, 11, 12] results in the thermo-dynamical destabilization of MgH_2 [8]. Notwithstanding that HEBM exhibits several advantages, drawbacks are also present due to powder processing, i.e. surface oxidation, large energy consumption, the necessity of an inert atmosphere, a potential fire risk and the difficulty of industrial level production.

These disadvantages of HEBM have extensively been eliminated very recently by novel bulk SPD techniques, including high-pressure torsion (HPT) [13-16], cold rolling [17-19] and equal-channel angular pressing [20-23]. These bulk methods have numerous benefits, i.e. the process is less intensive than HEBM, scaling up to larger quantities at a lower cost has a larger potential, impurity concentration is lower and causes less safety concerns [20].

Recently, an alternative SPD method was invented by Lu and coworkers by modifying the surface layer of a bulk material by mechanical attrition [24, 25]. Conventional surface-modified techniques usually involve chemical reactions resulting in an optimized mechanical, tribological or chemical structure of the surface layer in order to improve the general performance of the end-product. Nevertheless, the change of the surface microstructure by decreasing the grain size of the top-most layer of the bulk material can also accelerate the different reactions. Namely, the surface mechanical attrition treatment (SMAT) technique involves repeated multidirectional impacts by flying balls to induce severe plastic deformation in the surface layer of a target sample accompanied with large grain boundary misorientation, formation of dislocation blocks and surface nanocrystallization [26]. This nanocrystalline surface layer becomes chemically active, promoting the effectiveness of subsequent treatments such as nitriding [24] and chromizing [27]. Examination of the Mg alloy subjected to SMAT indicated an improved wear resistance of the surface nanocrystalline layer with an average grain size of 30±5 nm [28, 29]. As a result of the SMAT process, the micro-hardness of a biodegradable Mg-alloy has increased considerably in the near-surface region, however, the high dislocation density and abundant grain boundaries have severely weakened the corrosion resistance [30]. Cross sectional structural investigations revealed that the SMAT affected layer can be sub-divided into three zones, i.e. an ultrafine grain zone at the top surface, a subsurface transition zone and

* To whom all correspondence should be sent:
E-mail: reveszadam@ludens.elte.hu

a deformed zone where the initial grains are only plastically deformed [31]. The enhanced hardening achieved by the non-uniform deformation and grain-size gradient microstructure during the SMAT technique can satisfactorily be correlated by the physical model of Li et al. [32].

In the present experiment, we applied the SMAT technique on commercial Mg disks for different treatment times to generate a different microstructure in the severely deformed top layer. We demonstrate the correlation of hydrogen absorption kinetics and the microstructure obtained by applying the Convolutional Whole Profile Fitting (CMWP) algorithm of X-ray line profiles.

EXPERIMENTAL

SMAT processing

The mechanical treatment by the SMAT technique was carried out on commercial magnesium specimens (Goodfellow #MG007918) in a SPEX 8000 mixer mill. The conventional end cap of the container was replaced by a well-attached Mg disk target (50 mm in diameter and 5 mm in thickness). In order to ensure an approximately homogeneous distribution of the impacts, the stainless steel vial was filled with plenty hardened steel balls. Based on preliminary experiments [33], we applied 40 balls with a diameter of 6.35 mm and 12 balls with a diameter of 12.5 mm for different treatment times (15 min, 30 min and 90 min). The whole SMAT process was carried out in air. It is noted that the use of a few balls can lead to a non-uniform distribution of the impact points, while too many balls result in many ball-to-ball collisions and a reduced impact velocity.

Microstructural characterization

Microstructural characterization of the surface of the SMATed disks was performed by X-ray powder diffraction (XRD) with Cu-Kα radiation on a Philips X'pert powder diffractometer in θ-2θ geometry. The instrumental pattern was measured on NIST SRM660a LaB6 peak profile standard material.

The recorded X-ray diffraction patterns have been evaluated by the CMWP fitting procedure developed by prof. T. Ungár and co-workers [34]. Briefly, the CMWP analysis incorporates the direct fit of the whole of the X-ray diffractogram as measured by summing up the background, theoretically constructed profile functions and measured instrumental profile. These profile functions are calculated for each Bragg-reflection as the inverse Fourier transform of the product of the size and strain of Fourier coefficients and the Fourier coefficients of the corresponding measured instrumental profile [35]. In the simplest version of the CMWP analysis it is assumed that the crystallites are spherical and obey lognormal size distribution:

$$G(x) = (2\pi)^{-1/2}\,\sigma^{-1}\,x^{-1}\exp[-(\ln(x/m))^2/2\sigma^2]\,, \quad (1)$$

where σ and *m* are the variance and median of the distribution, respectively. Besides the microstructure size parameters, the line profile analysis provides the strain parameters, the average dislocation density (ρ) and effective outer cut-off radius of dislocations (R_e). From the available data, the average coherently scattering crystallite size can be determined [34] as:

$$\langle D\rangle = m\exp(2.5\sigma^2)\,, \quad (2)$$

More details of the fitting algorithm and its systematic application to ball-milled Mg-based powders can be found elsewhere [10, 35, 36].

The morphology was studied on a FEI QUANTA 3D dual beam scanning electron microscope (SEM). The local composition was quantitatively determined by energy dispersive X-ray (EDX) analysis.

Hydrogen sorption kinetics

Hydrogenation kinetic curves of the SMAT processed Mg samples were measured by a Sieverts'-type apparatus (PCT) at 573 K. The initial hydrogen pressure was set as 1 MPa. For details, see [15].

RESULTS AND DISCUSSION

The microstructural variations associated with the SMAT process of commercial Mg disks can be monitored in Fig. 1. The diffractograms carried out on the topmost surface of all treated states are evidently characterized by the peaks of hexagonal Mg (JCPDS 35-0821). As the milling commences, the breadth of the Bragg-peaks changes slightly, indicating a variation of lattice strain and average grain-size induced by the severe plastic deformation during the surface modification. In addition, faint diffraction peaks corresponding to the MgO phase emerge at the end of the treatment process. As a result of the surface treatment, one might expect some evolving anisotropy, nevertheless the relative intensities of the Mg-peaks change only negligibly, contrary to other different SPD-processed Mg-alloys [15, 23]. An example of the CMWP fitting procedure is presented in Fig. 2, where the measured diffractogram corresponding to

the sample SMATed for 15 min, the fitted pattern and the difference plot between the measured and fitted patterns are presented. An obvious correlation between the measured and fitted pattern is clear, however slight differences occur at the high intensity peak centers.

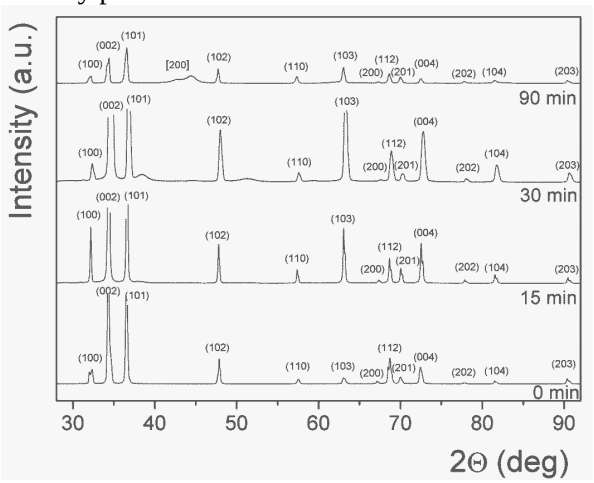

Fig. 1. XRD patterns taken from the surface of the Mg plates treated for different times. The brackets (…) and […] denote the Bragg-peaks of hexagonal Mg and MgO, respectively.

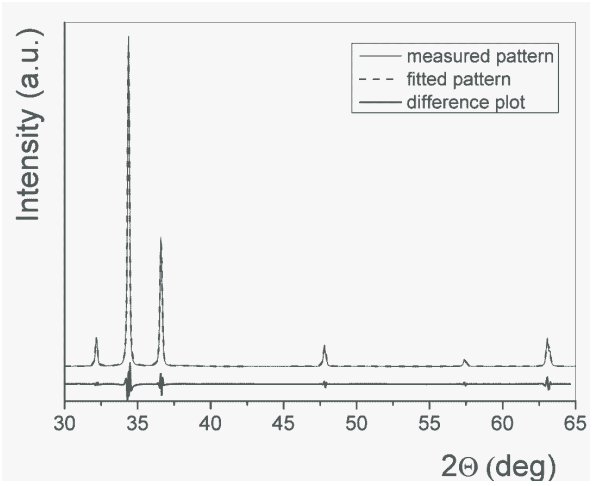

Fig. 2. Measured XRD pattern of the Mg disk SMATed for 15 min, the function fitted by the CMWP method and the difference between the measured and fitted data.

The median and the variance of the magnesium crystallite-size distribution as a function of the SMAT procedure time determined by the CMWP procedure can be realized in Fig. 3. As seen, the *m* value decreases continuously from the initial value of 29 nm to 18.5 nm at the early stages of the treatment time, however, a remarkable increase up to 32.4 nm is noticed after 90 min. At the same time, σ gradually decreases for up to 30 min from 0.74 to 0.58 and then obeys a subsequent increase (0.81) at the end of the SMAT treatment. From the calculated data of *m* and σ, the corresponding normalized log-normal distribution functions can be plotted, see Fig. 4. A simultaneous shift of the distribution maxima to lower values and a significant narrowing of the histograms up to 30 min of SMAT treatment are evidenced from the curves, indicating that not only a crystallite-size reduction occurs in the uppermost layers of the Mg disks, but a homogenization on the nanoscale also takes place. Surprisingly, these phenomena do not continue until the end of the SMAT process, on the contrary, longer treatment time exhibits a wider distribution of the crystallite size referring to a relatively more inhomogeneous microstructure. Moreover, the right-hand sidetail of the distribution function becomes more pronounced, corresponding to the formation of larger crystallites.

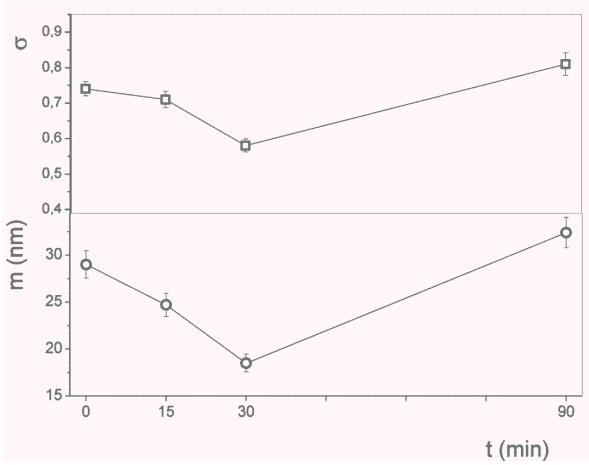

Fig. 3. Variation of the median (m) and the variance (σ) as a function of treatment time.

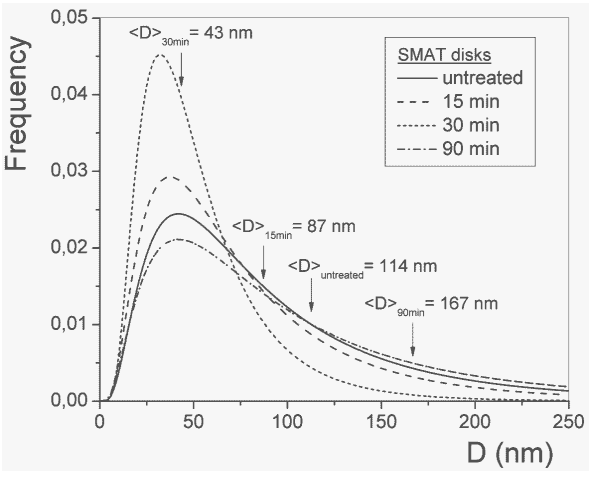

Fig. 4. Crystallite size distribution functions of the Mg disks. The volume averaged crystallite size ($\langle D \rangle = m \exp(2.5\sigma^2)$) for each treatment time is also denoted.

The calculated volume averaged crystallite size values ($\langle D \rangle$) are plotted in Fig. 5. As one can conclude, the SMAT process changes the microstructure of the top deformed layer considerably, $\langle D \rangle$ decreases by a factor of 3 (to 43

nm) after 30 min of treatment. Thereafter some kind of recrystallization takes place, reaching a final value of ⟨D⟩=167 nm. As described above, the CMWP analysis provides also the strain parameters, in our case the average lattice defect density, i.e. the dislocation density plays a crucial role. Fig. 5 also presents the variation of ρ as a function of the surface treatment time. A roughly linear increase can be noticed reaching a maximum value of $\rho=2.5*10^{13}$ m^{-2} after finishing the SMAT process. This value is slightly lower than that as found for ball-milled Mg powder [35] and an Mg-alloy processed by equal channel angular pressing [37]. Despite the large defect density, the obtained average defect distance L≥200 nm ($L=\rho^{-1/2}$) exceeds the average crystallite size ⟨D⟩ at any treated state. Consequently, a significant portion of the crystallites can be considered as defect-free. In addition, as obtained from the analysis, the severe plastic deformation during SMAT favors the formation of ⟨a⟩-type dislocations with a Burgers' vector $b=\frac{1}{3}\langle\bar{2}110\rangle$, exhibiting the lowest formation energy among the possible types of dislocations. The relative fraction of ⟨a+c⟩ and ⟨c⟩-type of dislocations is negligible.

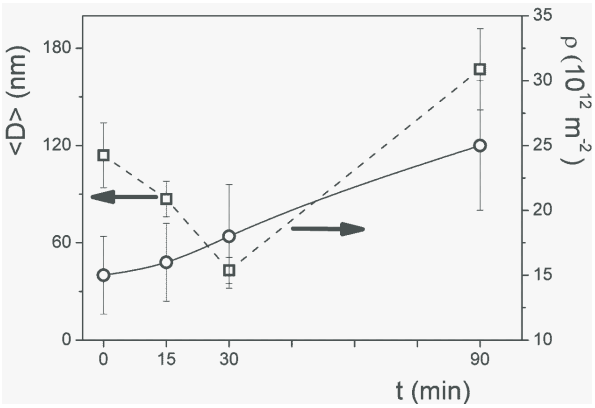

Fig. 5. Variation of the average crystallite size (⟨D⟩) and the average dislocation density (ρ) as a function of the SMAT treatment time.

SEM images taken on the cross-section of the sample SMATed for the longest treatment time (90 min) explain some aspects of the relevant XRD pattern and exhibit several interesting features concerning the morphology of the severely deformed top layer (Fig. 6). As the low magnification micrograph (250x) indicates, the surface of the treated sample is uneven, clear signs of surface shearing and folding are visible and can be divided up into well-separated areas of different contrast. In some areas the formation of a non-contiguous bright surface layer is observed. One might also notice that cracks perpendicular to the surface, which are favorable for accelerated hydrogen diffusion, penetrate into the bulk regions. At higher magnification (1000x) it is clear that the surface layer is not uniform, its thickness spans over a wide range with an average value of 22 μm. The results of the EDS elemental analysis carried out on three different regions (denoted by rectangles) can be found in Table 1.

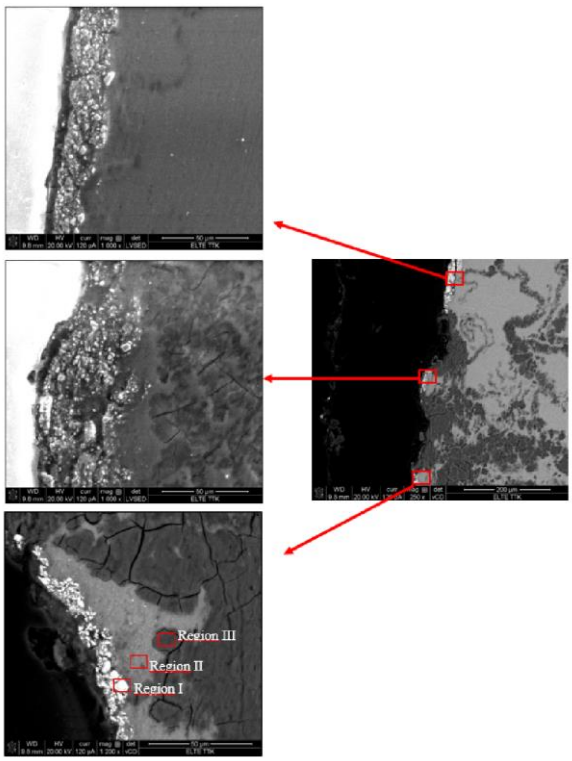

Fig. 6. SEM images taken on different parts of the cross section of the disk treated for 90 min.

Table 1. Elemental concentrations of the three different regions obtained on the cross section of the Mg disk treated for 90 min of SMAT.

Element	Region I	Region II	Region III
	Atomic percent		
Mg	76,41	99,10	99,75
Fe	20,93	0,33	0,14
Ni	1,85	0,10	0,04
Nb	0,66	0,23	0,07
Al	0,15	0,24	0,00

Concentrations averaged for the brightest white area (Region I) are significantly enriched in iron. Regions II and III are abundant in magnesium, the contrast difference may originate from the different iron and trace element content. At first glance, the detected high iron content at some positions of the surface layer is surprising, since no elemental Fe could be identified on the corresponding XRD pattern (see Fig. 1). Henceforth, it is assumed that iron is dissolved in the Mg-lattice and on the grain boundaries among the individual crystallites, even though Fe is immiscible in Mg according to the

equilibrium phase diagram [38]. Nevertheless, the extreme severe plastic deformation occurring at the contact points between the target and the balls may result in highly non-equilibrium processes that can promote some solubility of iron in Mg. The detected significant amount of iron presumably originates from the milling media, i.e. the steel vial and the balls. During the initial stages of the SMAT process the bombarded Mg-targets become harder and physically active. After a certain amount of processing time, the abundant ball-to-target collisions can induce some removal of hardened Mg particles (chips) from the top layer. Later on these particles are mixed with iron debris in the milling container due to the ball-to-ball collisions. As a final step, this powder mixture is re-depositied onto some parts of the fresh and active surface of the target disk forming the observed non-contiguous iron-rich top surface layer.

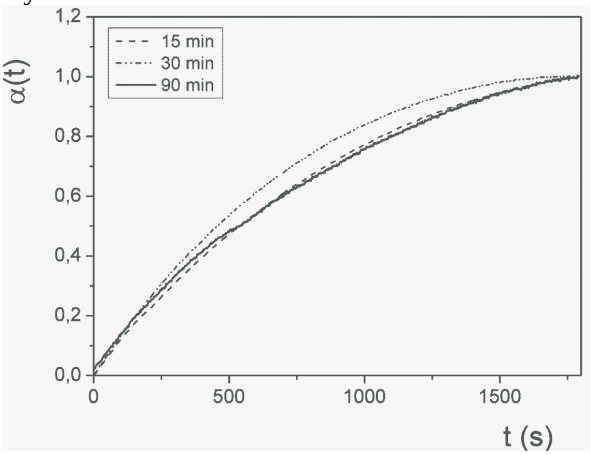

Fig. 7. Normalized hydrogen kinetic absorption curves of the Mg plates, treated for different SMAT times.

Normalized hydrogen absorption kinetic data (α) for the different Mg plates obtained at 573 K are presented in Fig. 7. All the specimens absorb hydrogen almost without activation, as the maximum capacity is reached after the first full absorption-desorption cycle. The detectable maximum capacity of the disks increases gradually with the SMAT treatment time, confirming the fact that Mg or Mg-based alloys processed by SPD under air are able to absorb hydrogen [39]. As one will also notice, the initial absorption kinetics is fast for all samples, reaching 50% of hydriding within 500s. As the CMWP results indicate (see Figs. 4 and 5), the specimen treated for the longest time (90 min) suffers a recrystallization of the nanocrystalline Mg-grains, however, it exhibits the largest defect density. Henceforth, the observed increase in the maximum H-capacity can be attributed mainly to the lattice defects (dislocations) generated during the heavy shear deformation during the SMAT process which can act as hydrogen absorption sites in the grain interiors by enhancing the diffusion of the H atoms, while the role of the grain boundaries and particle surfaces is remarkably less important. In a recent paper we have shown that abundant lattice defects have a crucial role in the creation of new and easily accessible hydrogen sites in Mg-Ni alloys produced by HPT [15]. Moreover, Horita and co-workers demonstrated noticeable hydrogen storage performance in coarse-grained $MgNi_2$ processed by HPT due to the intense anisotropic strain, although this compound possesses no measurable capacity under equilibrium conditions [13].

The normalized absorption curves for all treatment times can satisfactorily be fitted by the contracting volume function (CV) [40]. In brief, this model is valid when the nucleation starts at the surface of the particle and growth takes place from the surface into the bulk and the growth of the new phase occurs with a constant interface velocity. The kinetics can then be described by:

$$\alpha_{CV}(t,R) = 1-(1-k_{CV}t)^n, \quad (3)$$

where k_{CV} is a reaction constant and can be given as $k_{CV} = u/R$, where u is the velocity of the hydride metal interface motion and R is the average crystallite radius. n depends on the dimensionality of the growth, with n =3 for three-dimensional and n =2 for two-dimensional growth. The parameters obtained from the CV fits are listed in Table 2. As realized, the dimensionality parameter increases monotonously with the treatment time referring to a more isotropic hydride formation. The u value is significantly the greatest for the disk processed for 90 min of SMAT, indicating that the growth velocity of the hydride phase is the largest for this specimen, in accordance with the above findings, i.e. despite the larger average crystallite size, the abundant lattice defects account for the observed H-storage performance. In addition, we can further assume that iron as a catalyst can also influence the hydrogenation of the Mg-disks processed by the SMAT technique.

Table 2. Fitting parameters of the CV-model for different times.

Treatment time (min)	$k_{CV}\left(\frac{1}{s}\right)$	n	$u\left(\frac{nm}{s}\right)$
15	$(4{,}686\pm0{,}010)\cdot10^{-4}$	2,378±0,007	0,020±0,024
30	$(4{,}997\pm0{,}009)\cdot10^{-4}$	2,669±0,006	0,003±0,014
90	$(4{,}112\pm0{,}033)\cdot10^{-4}$	2,798±0,029	0,082±0,027

CONCLUSIONS

In this study commercial Mg disks were subjected to intense plastic deformation by SMAT. The CMWP analysis of X-ray line profiles revealed that the uppermost layer of the disks undergoes significant microstructural changes, i.e. the volume averaged coherent crystallite size reaches a minimum of ⟨D⟩=43 nm after 30 min of SMAT treatment, while a significant recrystallization takes place after that (⟨D⟩=167 nm). During this process, the removal of hardened Mg particles from the top layer occurs which are mixed with iron debris in the milling container later on. As a final step, this powder mixture is re-depositied onto the target disk forming a non-contiguous iron-rich top surface layer. Combined XRD and SEM experiments confirmed that iron forms a non-equilibrium solid solution in the Mg-lattice. At the same time the average lattice defect obeys a roughly linear increase up to a final value of $\rho=2.5*10^{13}$ m^{-2}. The hydrogen absorption curves of all the SMAT processed samples can satisfactorily be fitted by the CV function. By analyzing the fitting parameters, we found that the growth velocity of the hydride phase is the largest for the disk treated for 90 min, indicating that lattice defects (dislocations) generated during the SMAT process can act as hydrogen absorption sites in the grain interiors, while the role of the grain boundaries and particle surfaces is remarkably less important.

Acknowledgements: *Á.R. is indebted for the János Bolyai Research Scholarship of the Hungarian Academy of Sciences. T.S. is grateful to the FP7 project Beyond Everest. The authors appreciate the support of G. Varga in the SEM experiments. We acknowledge the support of the COST Action MP1103.*

REFERENCES

1. E.C.E. Rönnebro, E.H. Majzoub,*MRS Bull.*, **38**, 452(2013).
2. L. Schlapbach, A. Züttel, *Nature*, **414**, 353(2001).
3. R.A. Varin, T. Czujko, Z.S. Wronski,Nanomaterials for Solid State Hydrogen Storage, Springer Science, New York, 2009.
4. R.Z. Valiev, R.K. Ishlamgaliev, I.V. Alexandrov,*Prog. Mater. Sci.*,**45**, 103(2000).
5. Y. Estrin, A. Vinogradov, *Acta Mater.*, **61**, 782 (2013).
6. L. Zaluski, A. Zaluska, P. Tessier, J.O. Ström-Olsen, R. Schulz,*Mater. Sci. Forum*, **225**,853 (1996).
7. D. Fátay, Á. Révész, T. Spassov,*J. Alloys Compd.*,**399**, 237(2005).
8. W. Oelerich, T. Klassen, R. Bormann,*J. Alloys Compd*.,**315**, 237 (2001).
9. Á. Révész, D. Fátay, T. Spassov,*J. Alloys Compd.*,**434-435**, 725(2007).
10. D. Fátay, T. Spassov, P. Delchev, G. Ribárik, Á. Révész,*Int. J. Hydrogen Energy*, **32**, 2914 (2007).
11. X. Zhao, S. Han, Y. Zhu, X. Chen, D. Ke, Z. Wang, T. Liu, Y. Ma, *J. Solid State Chem.*, **221**, 441 (2015).
12. X. Zhu, L. Pei, Z. Zhao, B. Liu, S. Han, R. Wang, *J. Alloys Compd.*, **577**, 64 (2013).
13. Y. Kusadome, K. Ikeda, Y. Nakamori, S. Orimo, Z. Horita, *Scripta Mater.*, **57**, 751(2007).
14. K. Edalati, A. Yamamoto, Z. Horita, T. Ishihara,*Scripta Mater.*,**64**, 880 (2011).
15. Á. Révész, Zs. Kánya, T. Verebélyi, P.J. Szabó, A.P. Zhilyaev, T. Spassov, *J. Alloys Compd.*, **504**, 83 (2010).
16. T. Hongo, K. Edalati, H. Iwaoka, M. Arita, J. Matsuda, E. Akiba, Z. Horita, *Mater. Sci. Engineering A*, **618**, 1 (2014).
17. S.D. Vincent, J. Lang, J. Huot,*J. Alloys Compd.*, **512**, 290 (2012).
18. J. Bellemare, J. Huot,*J. Alloys Compd*.,**512**, 33 (2012).
19. D.R. Leiva, H.C. de Almeida Costa, J. Huot, T.S. Pinheiro, A.M. Jorge, T.T. Ishikawa, W.J. Botta, *Mater. Res.*, **15**, 813 (2012).
20. V.M. Skripnyuk, E. Rabkin, Y. Estrin, R. Lapovok,*Acta Mater.*, **52**, 405 (2004).
21. V.M. Skripnyuk, E. Rabkin, Y. Estrin, R. Lapovok,, *Int. J. Hydrogen Energy*, **34**, 6320 (2009).
22. A.M. Jorge, E. Prokofiev, G.F. de Lima, E. Rauch, M. Veron, W.J. Botta, M. Kawasaki, T.G. Langdon,*Int. J. Hydrogen Energy*, **38**, 8306 (2013).
23. Á. Révész, M. Gajdics, L.K. Varga, Gy.Krállics, T. Spassov, *Int. J. Hydrogen Energy*, **39**, 9911 (2014).
24. W.P. Tong, N.R. Tao, Z.B. Wang, J. Lu, K. Lu, *Science*, **299**, 686 (2003).
25. X. Wu, N. Tao, Y. Hong, G. Liu, B. Xu, J. Lu, K. Lu, *Acta Mater*.,**53**, 681(2005).
26. N.R. Tao, Z.B. Wang, W.P. Tong, M.L. Sui, J. Lu, K. Lu, *Acta Mater.*, **50**, 4603 (2002).
27. Z.B. Wang, J. Lu, K. Lu, *Acta Mater.*,**53**, 2081 (2005).
28. H.Q. Sun, Y.N. Shi, M.X. Zhang, *Surf. Coat. Technol.*, **202**, 2859 (2008).
29. H.Q. Sun, Y.N. Shi, M.X. Zhang, K. Lu, *Surf. Coat. Technol.*, **202**, 3947 (2008).
30. N. Li, Y.D. Li, Y.X. Li, Y.H. Wu, Y.F. Zheng, Y. Han, *Mater. Sci. Engineering C*, **35**, 314 (2014).
31. Y. Samih, B. Beausir, B. Bolle, T. Grosdidier, *Mater. Charact.*, **83**, 129 (2013).
32. J. Li, S. Chen, X. Wu, A.K. Soh, *Mater. Sci. Engineering A*,**620**, 16 (2015).
33. Á. Révész, L. Takacs, *J. Alloys Compd.*, **441**, 111 (2007).
34. G. Ribárik, J. Gubicza, T. Ungár, *Mater. Sci. Engineering A*,**387-389**, 343 (2004).35. Á. Révész, D. Fátay,*J. Power Sources*, **195**, 6997 (2010).
35. Á. Révész, M. Gajdics, T. Spassov, *Int. J. Hydrogen Energy*, **38**, 8342 (2013).
36. J. Gubicza, K. Máthis, Z. Hegedűs, G. Ribárik, A.L. Tóth, *J. Alloys Compd.*, **492**, 166 (2010).

37. A. A. Nayeb-Hashemi, J. B. Clark, L. J. Swartzendruber, *Bulletin of Alloy Phase Diagrams*, **6**, 235 (1985).
38. J. Huot, S.D. Vincent,*J. Alloys Compd*., **509**, L175 (2011).
39. P.W.M Jacobs and F.C Tompkins: Classification and theory of solid reactions, in Chemistry of the Solid State, W.E. Garner (ed.), Butterworth, London, 1955, p.184..

СОРБЦИЯ НА ВОДОРОД В МАГНЕЗИЕВИ ПЛАСТИНИ ДЕФОРМИРАНИ ЧРЕЗ ПОВЪРХНОСТНО МЕХАНИЧНО ИЗТРИВАНЕ

А. Ревеш [1], Ц. Силаги [1], Т.Спасов [2]

[1]Факултет по физика на материалите, Йотвош университет, Будапеща, H-1518, P.O.B. 32, Унгария
[2]Факултет по химия и фармация, Софийски университет "Св. Кл. Охридски", 1 Дж. Баучер, 1164 София, България

Получена на 26 юни 2015 г., коригирана на 1 декември 2015 г.

(Резюме)

Търговски магнезиеви дискове са модифицирани чрез повърхностно механично изтриване в мелница тип SPEX 8000. Морфологичните и микроструктурни промени по време на процеса на пластична деформация са изследвани с помощта съответно на сканираща електронна микроскопия и рентгеново дифракционен линеен профилен анализ. Водородно-абсорбционни експерименти с апарат на Сиверт показват наличие на корелация между кинетиката на водородна сорбция и микроструктурните параметри на материала.